Microglial Activation and Connectivity in Alzheimer Disease and Aging

Boris-Stephan Rauchmann, MD, MHBA [1,2,3,4] Matthias Brendel, MD, MHBA [5,6] Nicolai Franzmeier, PhD [7] Lena Trappmann,[1] Mirlind Zaganjori,[1] Ersin Ersoezlue,[1] Estrella Morenas-Rodriguez, PhD,[2,8] Selim Guersel,[1,2] Lena Burow, MSc,[1] Carolin Kurz, MD,[1] Jan Haeckert, MD,[1,9] Maia Tatò, MD,[1] Julia Utecht, MD,[1] Boris Papazov, MSc,[10] Oliver Pogarell, MD,[1] Daniel Janowitz, MD,[7] Katharina Buerger, MD,[2,7] Michael Ewers, PhD [7] Carla Palleis, MD,[2,6,11] Endy Weidinger, MD,[11] Gloria Biechele,[5] Sebastian Schuster,[5] Anika Finze,[5] Florian Eckenweber, MD,[5] Rainer Rupprecht, MD,[12] Axel Rominger, MD,[5,13] Oliver Goldhardt, MD [14] Timo Grimmer, MD,[14] Daniel Keeser, PhD,[1,4,10] Sophia Stoecklein, MD [10] Olaf Dietrich, PhD,[10] Peter Bartenstein, MD,[5,6] Johannes Levin, MD,[2,6,11] Günter Höglinger, MD,[2,15] and Robert Perneczky, MD, MBA[1,2,3,4,6,16]

Objective: Alzheimer disease (AD) is characterized by amyloid β (Aβ) plaques and neurofibrillary tau tangles, but increasing evidence suggests that neuroinflammation also plays a key role, driven by the activation of microglia. Aβ and tau pathology appear to spread along pathways of highly connected brain regions, but it remains elusive whether microglial activation follows a similar distribution pattern. Here, we assess whether connectivity is associated with microglia activation patterns.

Methods: We included 32 Aβ-positive early AD subjects (18 women, 14 men) and 18 Aβ-negative age-matched healthy controls (10 women, 8 men) from the prospective ActiGliA (Activity of Cerebral Networks, Amyloid and Microglia in Aging and Alzheimer's Disease) study. All participants underwent microglial activation positron emission tomography (PET) with the third-generation mitochondrial 18 kDa translocator protein (TSPO) ligand [^{18}F]GE-180 and magnetic resonance imaging (MRI) to measure resting-state functional and structural connectivity.

Results: We found that inter-regional covariance in TSPO-PET and standardized uptake value ratio was preferentially distributed along functionally highly connected brain regions, with MRI structural connectivity showing a weaker

View this article online at wileyonlinelibrary.com. DOI: 10.1002/ana.26465

Received Apr 5, 2022, and in revised form Jul 27, 2022. Accepted for publication Jul 28, 2022.

Address correspondence to Dr Perneczky, Division of Mental Health of Older Adults, Department of Psychiatry and Psychotherapy, Ludwig-Maximilians-Universität München, Nußbaumstr 7, 80336 Munich, Germany. E-mail: robert.perneczky@med.lmu.de

From the [1]Department of Psychiatry and Psychotherapy, University Hospital, Ludwig Maximilian University of Munich, Munich, Germany; [2]German Center for Neurodegenerative Diseases, Munich, Germany; [3]Sheffield Institute for Translational Neuroscience, University of Sheffield, Sheffield; [4]Department of Neuroradiology, University Hospital, Ludwig Maximilian University of Munich, Munich, Germany; [5]Department of Nuclear Medicine, University Hospital, Ludwig Maximilian University of Munich, Munich, Germany; [6]Munich Cluster for Systems Neurology, Munich, Germany; [7]Institute for Stroke and Dementia Research, University Hospital, Ludwig Maximilian University of Munich, Munich, Germany; [8]Chair of Metabolic Biochemistry, Biomedical Center, Faculty of Medicine, Ludwig Maximilian University of Munich, Munich, Germany; [9]Department of Psychiatry, Psychotherapy, and Psychosomatics, University of Augsburg, Augsburg, Germany; [10]Department of Radiology, University Hospital, Ludwig Maximilian University of Munich, Munich, Germany; [11]Department of Neurology, University Hospital, Ludwig Maximilian University of Munich, Munich, Germany; [12]Department of Psychiatry and Psychotherapy, University of Regensburg, Regensburg, Germany; [13]Department of Nuclear Medicine, University of Bern, Inselspital, Bern, Switzerland; [14]Department of Psychiatry and Psychotherapy, Rechts der Isar Hospital, Technical University of Munich, Munich, Germany; [15]Department of Neurology, Hannover Medical School, Hannover, Germany; and [16]Ageing Epidemiology Research Unit, School of Public Health, Imperial College London, London

Additional supporting information can be found in the online version of this article.

association with microglial activation. AD patients showed increased TSPO-PET tracer uptake bilaterally in the anterior medial temporal lobe compared to controls, and higher TSPO-PET uptake was associated with cognitive impairment and dementia severity in a disease stage-dependent manner.
Interpretation: Microglial activation distributes preferentially along highly connected brain regions, similar to tau pathology. These findings support the important role of microglia in neurodegeneration, and we speculate that pathology spreads throughout the brain along vulnerable connectivity pathways.

ANN NEUROL 2022;00:1–14

Extracellular amyloid β (Aβ) plaques and intracellular neurofibrillary tau tangles are the pathological hallmarks of Alzheimer disease (AD), leading to a cascade of brain changes resulting in cognitive decline and dementia.[1] Recent genetic, molecular, and clinical evidence suggests that neuroimmune mechanisms are associated with AD risk and contribute to disease progression.[2,3] Patients with symptomatic AD show alterations in cerebrospinal fluid (CSF) and blood pro- and anti-inflammatory proteins,[4,5] including the soluble triggering receptor expressed on myeloid cells 2 (sTREM2), a marker of activated microglia,[6] typically surrounding Aβ plaques as the brain's main innate immune response.[7] This suggests that neuroinflammation and microglial activation play a key role in the pathogenesis of AD.

In vivo, microglial activation can be measured with positron emission tomography (PET) tracers targeting the mitochondrial 18 kDa translocator protein (TSPO), located on the outer mitochondrial membrane and overexpressed on activated immune cells.[8] Increased microglial activation is apparent on TSPO-PET scans in different neurodegenerative disorders, including AD, corticobasal syndrome, and progressive supranuclear palsy.[3,9,10] Neuroinflammation, extracellular Aβ plaques, and intracellular tau neurofibrils seem to be linked closely. Within the microglia population, two distinct expression profiles were recently identified, associated with either Aβ load or tissue phosphorylated tau (ptau).[11] Colocalization of tau and activated microglia was demonstrated,[12,13] and Aβ plaque-dependent microglia was identified.[14] Furthermore, TSPO-PET binding correlates with increasing Aβ accumulation in AD mouse models,[15] and microglial activation may also act as a link between Aβ and tau pathology.[16]

Several studies in AD have demonstrated that changes in functional magnetic resonance imaging (fMRI) connectivity are associated with hallmark protein aggregations. Highly connected hub regions show increased tau accumulation on PET imaging, accelerated by Aβ pathology,[17] supporting a model of transneuronal spread of tau molecules.[18,19] Increasing evidence indicates that the spread of tau tangles in the neocortex is accompanied by microglial activation,[13,20] with both types of pathologies seemingly following a Braak-stage-like distribution pattern along an activated network of microglia, suggesting that Aβ and microglia together initiate tau spreading across the brain.[21,22]

The main aim of the present study was to explore whether connected brain regions show correlated TSPO-PET tracer uptake patterns, to identify the brain structural and functional network connectivity correlates of the cerebral neuroimmune response against AD. We used data, including TSPO-PET microglial activation, diffusion tensor imaging (DTI) structural connectivity, and MRI functional connectivity, from the prospective Activity of Cerebral Networks, Amyloid and Microglia in Aging and Alzheimer's Disease (ActiGliA) study to address our hypotheses. We speculate that microglial activation in AD spreads along connected brain areas, similar to a pattern observed for the prionlike spatial propagation of tau pathology.

Subjects and Methods

Study Design and Participants

The data used in this study originate from the baseline dataset of the ActiGliA study, a prospective, longitudinal, observational, single-center study of the Munich Cluster for Systems Neurology at Ludwig Maximilian University of Munich (LMU), initiated in 2017. Participants were recruited through specialized outpatient clinics at the LMU hospital Department of Psychiatry and Psychotherapy, Department of Neurology, Institute of Stroke and Dementia Research, and the Department of Psychiatry and Psychotherapy of the Technical University of Munich. ActiGliA comprises comprehensive neurocognitive, clinical, and lifestyle assessments based on the German Center for Neurodegenerative Disorders (DZNE) Longitudinal Cognitive Impairment and Dementia study[23]; MRI and PET imaging using tracers for Aβ and TSPO; and fluid biobanking, including CSF, plasma, serum, saliva, DNA, RNA, and peripheral blood mononuclear cells. Patients with early AD (subjective cognitive impairment, mild cognitive impairment, and mild AD dementia) and corticobasal syndrome (CBS)[24] and age-matched cognitively normal controls were included after providing written informed consent in line with the declaration of Helsinki. The study was approved by the ethics committee of LMU (project numbers 17-755 and 17-569).

Of 140 ActiGliA participants, all consecutive cases meeting the inclusion criteria for the present analyses were included, resulting in a cohort of n = 32 early AD patients and n = 18 cognitively normal controls. Ninety participants were not considered for the present analysis due to a diagnosis of CBS (n = 50) or other non-AD disorder (n = 23). Sixteen participants were excluded because of missing neuropsychological test results, and 1 participant was excluded because of extensive white matter lesions (Supplementary Figure 1). Cognitively normal controls

were defined as participants without cognitive impairment (Clinical Dementia Rating [CDR] global score = 0, Consortium to Establish a Registry for Alzheimer's Disease Neuropsychological Battery [CERAD-NB] total score ≥ 69,[25] and no indication of Aβ pathology on PET [negative visual read] and/or CSF examination [normal Aβ42/40 ratio as defined below]). AD continuum was defined as CDR global score ≥ 0.5, CERAD-NB total score ≤ 84, and presence of Aβ pathology on PET and/or CSF examination.

Clinical Assessments

The CDR, CERAD-NB,[26] and Mini-Mental State Examination (MMSE)[27] were conducted by trained psychologists at the LMU hospital memory clinic. Using the CERAD-NB, a total score was created as shown previously, comprising the 6 subtests semantic fluency (animals/60 seconds), modified Boston Naming Test, Word List Learning, Constructional Praxis, Word List Recall, and Word List Recognition Discriminability, with higher scores indicating better performance (maximum total score = 100).[25]

Genetic Polymorphisms

TSPO and apolipoprotein E (*APOE*) genotyping was performed at the Departments of Psychiatry and Psychotherapy of University of Regensburg and LMU, respectively. Genomic DNA was extracted from whole blood using a SQ Blood DNA kit from Omega Bio-Tek (Norcross, GA) according to the manufacturer's protocol. DNA quality was assessed by optical absorbance and gel electrophoresis. TaqMan quantitative polymerase chain reaction assays were used for amplification and Sanger method for sequencing.

Binding affinity of the [^{18}F]GE-180 TSPO ligand is affected by the codominant rs6971 (Ala/Thr) single nucleotide polymorphisms (SNPs) of the *TSPO* gene and needs to be considered in the imaging analysis.[28] High-affinity binders (HABs) are Ala/Ala carriers, low-affinity binders (LABs) are Thr/Thr carriers, and mixed-affinity binders (MABs) are Ala/Thr carriers. Only HABs and MABs were included in the PET analyses, with 6 LABs excluded. All TSPO-PET analyses were adjusted for binding status. The exclusion of LABs is justified by previous findings by our group, where we demonstrated a significant lower binding of [18F]GE-180-PET in LABs compared to

TABLE: Sociodemographic, Clinical, and Biomarker Characteristics of the Cohort

Characteristic	CN	AD Patients	*p*
Age, yr (SD)	69.22 (7.53)	71.31 (7.52)	0.35
Sex, F (%)	10/18 (56%)	18/32 (56%)	0.60
Weight, kg (SD)	76.39 (17.23)	69.50 (13.78)	0.13
Education, yr (SD)	14.83 (3.97)	14.81 (4.13)	0.99
CDR SOB (SD)	0.06 (0.16)	3.16 (1.73)	<0.001
CERAD-NB (SD)	86.42 (5.93)	58.53 (14.05)	<0.001
MMSE (SD)	29.28 (1.07)	24.25 (3.17)	<0.001
CSF Aß42, pg/ml (SD)	1,060.41 (482.93)	465.96 (167.51)	<0.001
CSF Aβ42/40 ratio (SD)	7.48 (1.01)	3.58 (0.96)	<0.001
CSF ptau181, pg/ml (SD)	49.75 (17.39)	102.17 (46.78)	<0.001
CSF ttau, pg/ml (SD)	230.37 (105.57)	635.21 (606.34)	0.009
CSF sTREM2, ng/ml (SD)	10.35 (3.00)	11.31 (3.49)	0.37
TSPO-PET SUVR (SD)	0.94 (0.04)	1.08 (0.08)	<0.001
APOE ε4 allele carriers (%)	4/18 (22%)	23/29 (79%)	<0.001
rs6971 binding status (%)	15/18 (83%) MAB 3/18 (17%) HAB	6/30 (20%) LAB 15/30 (50%) MAB 9/30 (30%) HAB	0.041

AD = Alzheimer disease; *APOE* = apolipoprotein E; Aβ42 = amyloid β 42; Aβ42/40 ratio = ratio Aβ42 to Aβ40; CDR SOB = Clinical Dementia Rating Sum of Boxes; CERAD-NB = Consortium to Establish a Registry for Alzheimer's Disease Neuropsychological Battery total score; CN = cognitively normal controls; CSF = cerebrospinal fluid; F = female; HAB = high-affinity binder; LAB = low-affinity binder; MAB = mixed-affinity binder; MMSE = Mini-Mental Status Examination; PET = positron emission tomography; ptau = phosphorylated tau protein; SD = standard deviation; sTREM2 = soluble triggering receptor expressed on myeloid cells 2; SUVR = standardized uptake value ratio; TSPO = mitochondrial 18 kDa translocator protein; ttau = total tau protein.

MABs and HABs.[29] Furthermore, data in this study showed higher [18F]GE-180-PET binding in HABs compared to MABs, although not significantly. To avoid possible confounding, we controlled our analysis for HAB and MAB binding status. The two SNPs rs429358 and rs7412 defining the *APOE* ε2, ε3, and ε4 alleles were analyzed to determine the *APOE* genotype. Sequencing data were analyzed using SnapGene software (GSL Biotech; www.snapgene.com). Participants were dichotomized into carriers versus noncarriers of the ε4 allele.

CSF Analyses

CSF peptide measures were generated from aliquoted samples using commercially available (Fujirebio, Malvern, PA) enzyme-linked immunosorbent assays (ELISAs). Aβ positivity was defined as a CSF Aβ42/40 ratio of <5.5%, as suggested previously.[30] Concentrations of total tau (ttau) and ptau181 were measured in CSF using the Innotest htau-Ag, and Innotest P-tau (181P) ELISA assays (Fujirebio Europe, Ghent, Belgium). The CSF sTREM2 concentrations were measured at the DZNE Munich based on previously established in-house ELISA protocols using duplicate samples.[31] Average measurements of the duplicates were used for the statistical analyses after applying method and plate-specific correction procedures.

MRI Acquisition and Preprocessing

MRI data for the entire ActiGliA cohort were acquired at the Department of Radiology of LMU on a 3T Magnetom Skyra MR system (Siemens Healthineers, Erlangen, Germany). A 0.8cm isovoxel high-resolution T1-weighted structural MRI sequence (repetition time [TR] = 2060 milliseconds, echo time [TE] = 2.17 milliseconds, flip angle [FA] = 12°, field of view [FoV] = 240mm), a diffusion-weighted imaging MRI sequence with a multiband acceleration factor of 3 (TR = 3,800 milliseconds, TE = 104.8 milliseconds, b-value = 2,000 s/mm^2, 108 diffusion directions, FA = 90°, FoV = 240mm), and a 2.5mm, 10-minute 32-second resting-state fMRI sequence with multiband acceleration factor of 6 (TR = 780 milliseconds, TE = 33 milliseconds, FA = 50°, FoV = 210mm) were acquired.

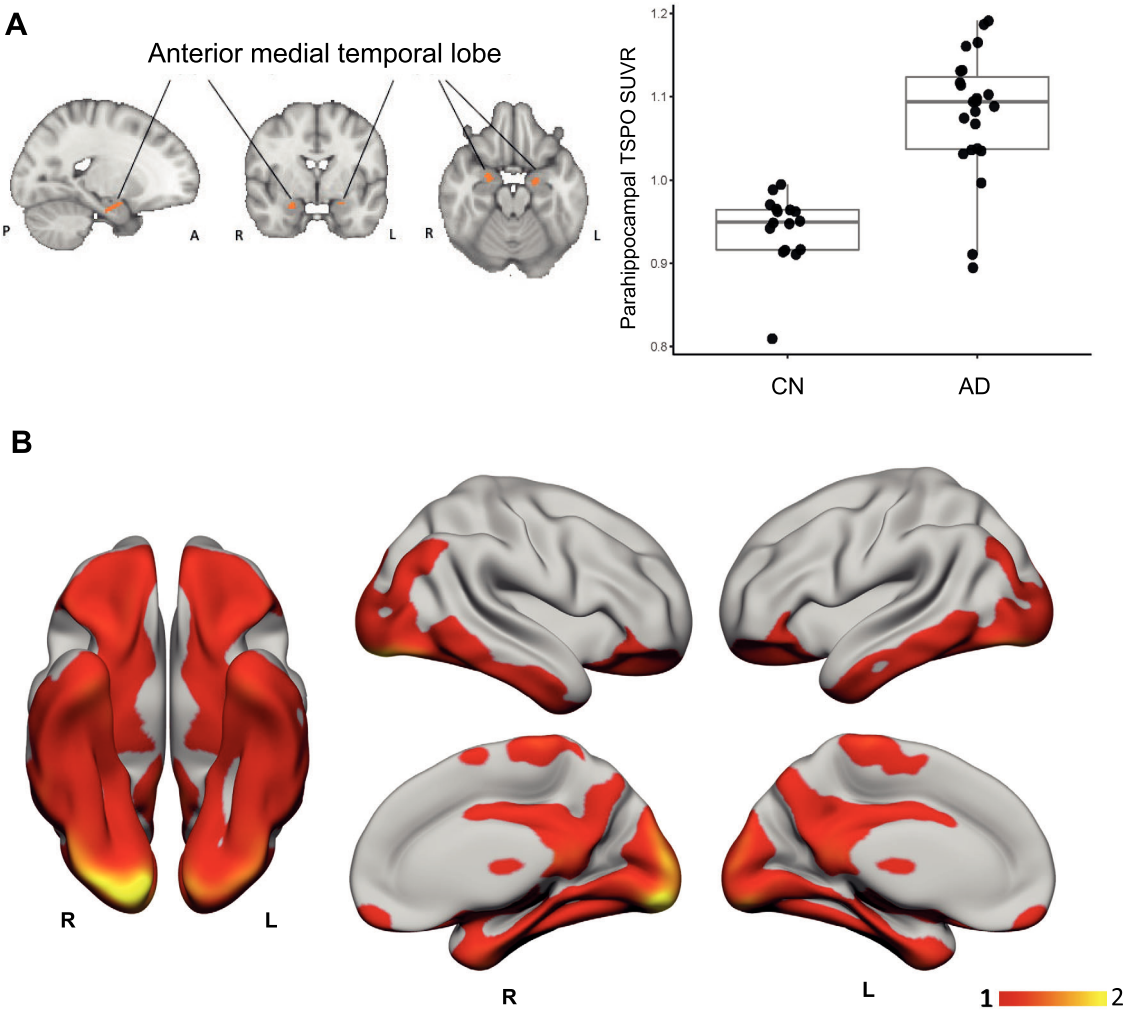

FIGURE 1: (A) Voxelwise group comparisons between Alzheimer disease (AD) and cognitively normal controls (CN; $p < 0.001$). Scatterplot shows individual and mean differences between patients and CN in mitochondrial 18 kDa translocator protein (TSPO) standardized uptake value ratio (SUVR). (B) Distribution of the mean SUVR TSPO-PET binding pattern within the AD group. L, left; R, right.

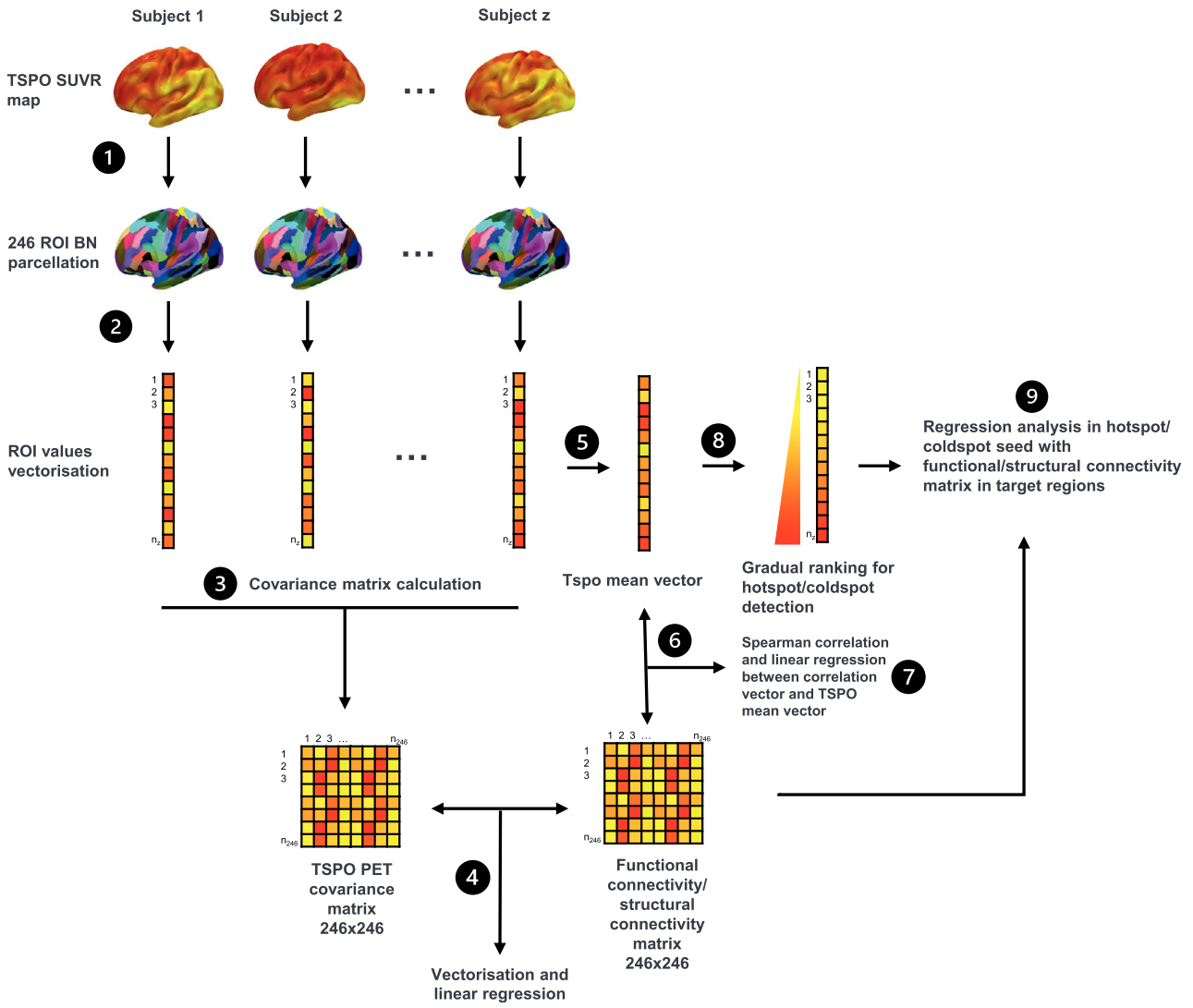

FIGURE 2: Figurative analysis workflow overview. (1) After preprocessing, individual mitochondrial 18 kDa translocator protein (TSPO)–positron emission tomography (PET) standardized uptake value ratio (SUVR) maps were parcellated based on the Brainnetome (BN) atlas. (2) Next, the parcellation based TSPO-PET SUVR for each subject was concatenated, vectorized, and *z*-transformed to remove intersubject differences of the tracer uptake, (3) followed by a pairwise interregional correlation to calculate a TSPO-PET covariance adjacency matrix for each diagnostic group. (4) To predict TSPO-PET covariance from structural/functional connectivity, the TSPO-PET and the resting state functioncal magnetic resonance imaging and diffusion tensor imaging magnetic resonance imaging-derived mean adjacency connectivity matrices were vectorized, and a linear regression analysis was performed. (5) A mean TSPO vector was calculated and (6) correlated with the mean adjacency matrix of functional and structural connectivity matrix. (7) In a linear regression analysis, the association between TSPO-PET and the correlation vector between functional/structural connectivity and TSPO SUVR was tested. (8) Identification of the TSPO-PET hot and cold spot regions by rank sorting the mean TSPO SUVR uptake vector for the 246 BN regions. (9) Analysis of the associations between TSPO-PET uptake in functional/structural connectivity target regions and the functional/structural connectivity in hot spot and cold spot seed areas by regression analysis between TSPO-PET uptake in all target regions and functional/structural connectivity in the identified hot spot/cold spot region. ROI = region of interest.

Resting-state functional connectivity was analyzed using the CONN fMRI functional connectivity toolbox (v17, www.nitrc.org/projects/conn) in MATLAB (MathWorks, Natick, MA). Preprocessing comprised visual inspection, volume-based fMRI analyses including realignment, slice-time correction, segmentation, and structural and functional normalization, artifact detection tools-based outlier detection, and functional smoothing using a 6mm kernel. The pipeline details can be found elsewhere (https://web.conn-toolbox.org/fmri-methods/preprocessing-pipeline). All DTI images were visually inspected. Preprocessing was performed using ExploreDTI,[32] a MATLAB toolbox, including motion correction and eddy current correction and correction for echo planar imaging distortions.

PET Acquisition and Preprocessing

Patients were scanned at the Department of Nuclear Medicine of LMU on a Biograph 64 PET/computed tomography (CT) scanner (Siemens Healthineers). Prior to PET acquisition,

a low-dose CT scan was acquired for attenuation correction. Emission data were acquired dynamically over 90 minutes or statically (time frame after tracer injection to calculate the standardized uptake value was 60–80 minutes) starting with the injection of 189 ± 12MBq [^{18}F]GE-180 as an intravenous bolus. The specific activity was on average 1.714 ± 523GBq/μmol at the end of radiosynthesis, and the injected mass was 0.13 ± 0.05nmol (based on n = 5 syntheses). Images were reconstructed using a 3-dimensional ordered subsets expectation maximization algorithm (16 iterations, 4 subsets, 4mm Gaussian filter) with a matrix size of 336 × 336 × 109 and a voxel size of 1.018 × 1.018 × 2.027mm. Standard corrections for attenuation, scatter, decay, and random counts were applied.

TSPO-PET scans were coregistered to the subject's individual T1-weighted structural MRI scan, and skull-stripped using FMRIB Software Library Brain Extraction Tool. Nonlinear spatial normalization parameters to the Montreal Neurological Institute (MNI) standard space were estimated using Advanced Normalization Tools. The obtained spatial normalization parameter estimations were subsequently used to normalize the TSPO-PET scan to the MNI space. To obtain standardized uptake value ratios (SUVRs), the TSPO-PET scans were intensity-normalized using the inferior cerebellar gray matter as reference region.[33] Follow-up acquisitions of the ActiGliA study include tau-PET imaging with PI-2620. For PI-2620, it was shown that an inferior cerebellar reference tissue reduced sources of spill over when compared to whole cerebellum.[34] To align reference tissues across tracers for upcoming analyses, we decided to stick to a unified reference tissue.

Analysis of TSPO-PET Differences between Diagnostic Groups

Differences between the diagnostic groups were estimated in a voxelwise analysis using SPM12 (Wellcome Centre for Human Neuroimaging, London, UK). MNI-normalized TSPO-PET images were spatially smoothed using an 8mm full width at half maximum kernel. In an atlas-based analysis, the individual TSPO tracer uptake was calculated in the regions of the Brainnetome (BN) atlas, a multimodal connectivity-based parcellation framework atlas based on a 246-region brain parcellation, including 210 cortical and 36 subcortical subregions.[35]

Analysis of the Structural and Functional Connectomes and Their Associations with TSPO-PET Covariance

The BN atlas was used to determine the individual in vivo connectivity architecture when assessing structural and functional connectivity. Group differences in functional and structural

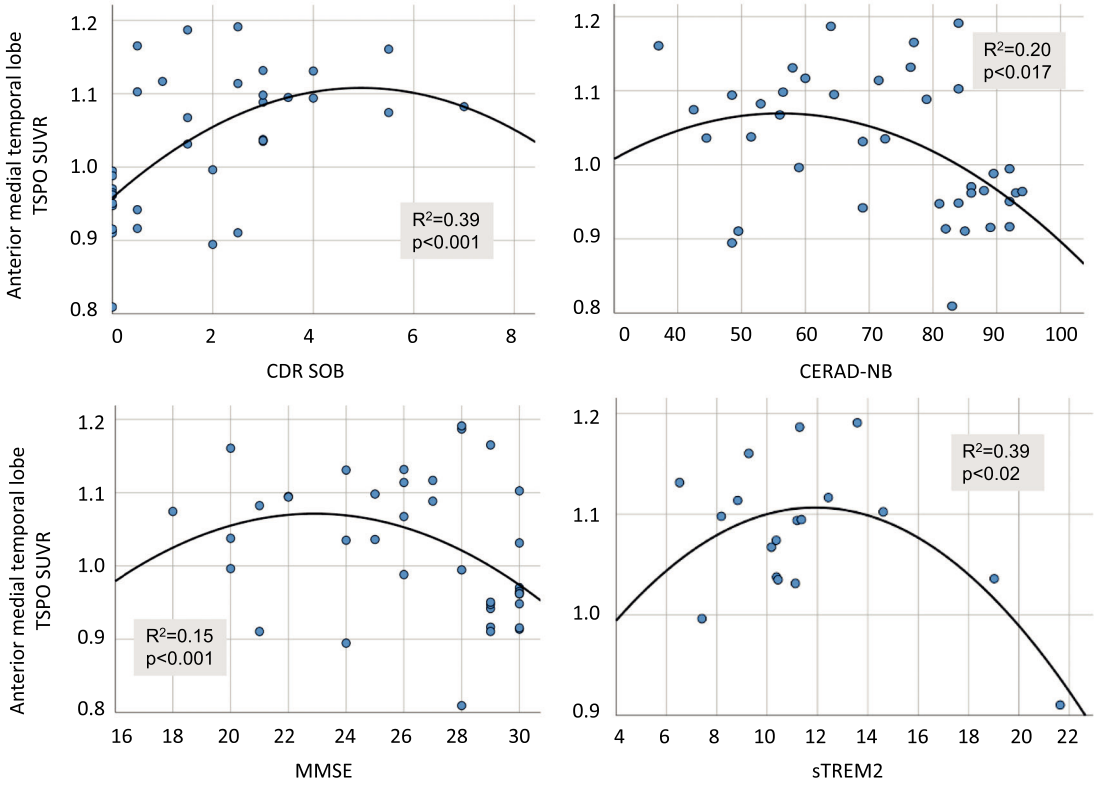

FIGURE 3: Associations of dementia severity and cognitive impairment with anterior medial temporal lobe mitochondrial 18 kDa translocator protein (TSPO)–positron emission tomography (PET) uptake in the whole study cohort and associations between cerebrospinal fluid soluble triggering receptor expressed on myeloid cells 2 (sTREM2) concentration and anterior medial temporal lobe TSPO-PET uptake in Alzheimer disease. CDR SOB = Clinical Dementia Rating Sum of Boxes; CERAD-NB = Consortium to Establish a Registry for Alzheimer's Disease Neuropsychological Battery total score; MMSE = Mini-Mental Status Examination; SUVR = standardized uptake value ratio.

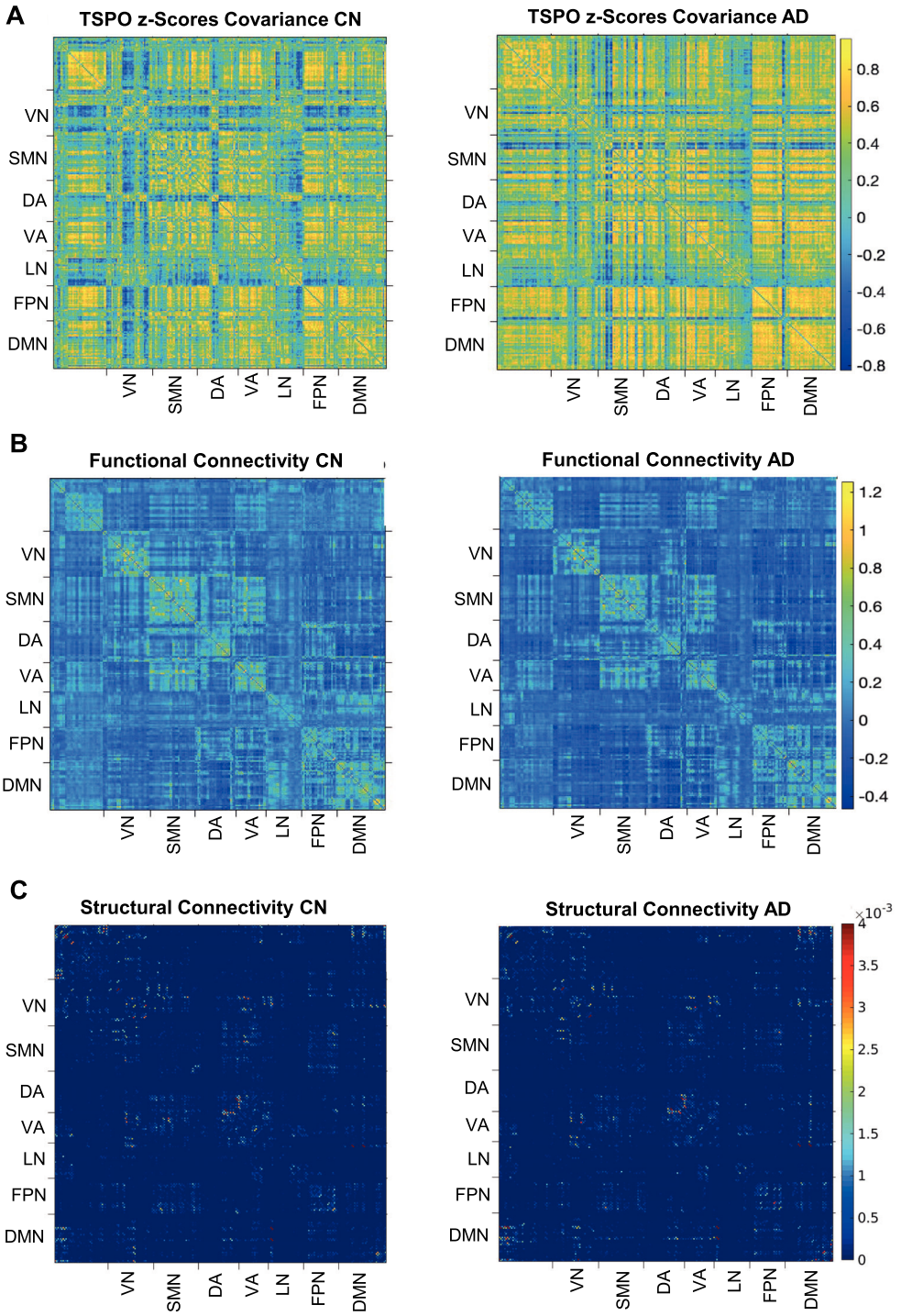

FIGURE 4: (A) Mitochondrial 18 kDa translocator protein (TSPO)–positron emission tomography covariance matrix of cognitively normal controls (CN) and Alzheimer disease (AD) patients. (B) Mean adjacency matrix of functional connectivity. (C) Mean adjacency matrix of structural connectivity. DA = dorsal attention network; DMN = default mode network; FPN = frontoparietal network; LN = limbic network; SMN = sensorimotor network; VA = ventral attention network; VN = visual network.

connectivity between AD and control subjects were assessed using the CONN toolbox and GraphVar.[36] The associations between TSPO-PET tracer uptake and functional and structural connectivity were analyzed using in-house MATLAB scripts for *z*-scaling, covariance calculation, and linear regression analysis. A figurative analysis workflow overview is presented in Figure 2.

Statistical Analyses

Group differences in functional connectivity were tested in a general linear model using individual adjacency matrices of the BN atlas-based 246-region parcellation in a region of interest (ROI)-to-ROI analysis in the CONN toolbox. All results were adjusted for age, sex, and education with false discovery rate

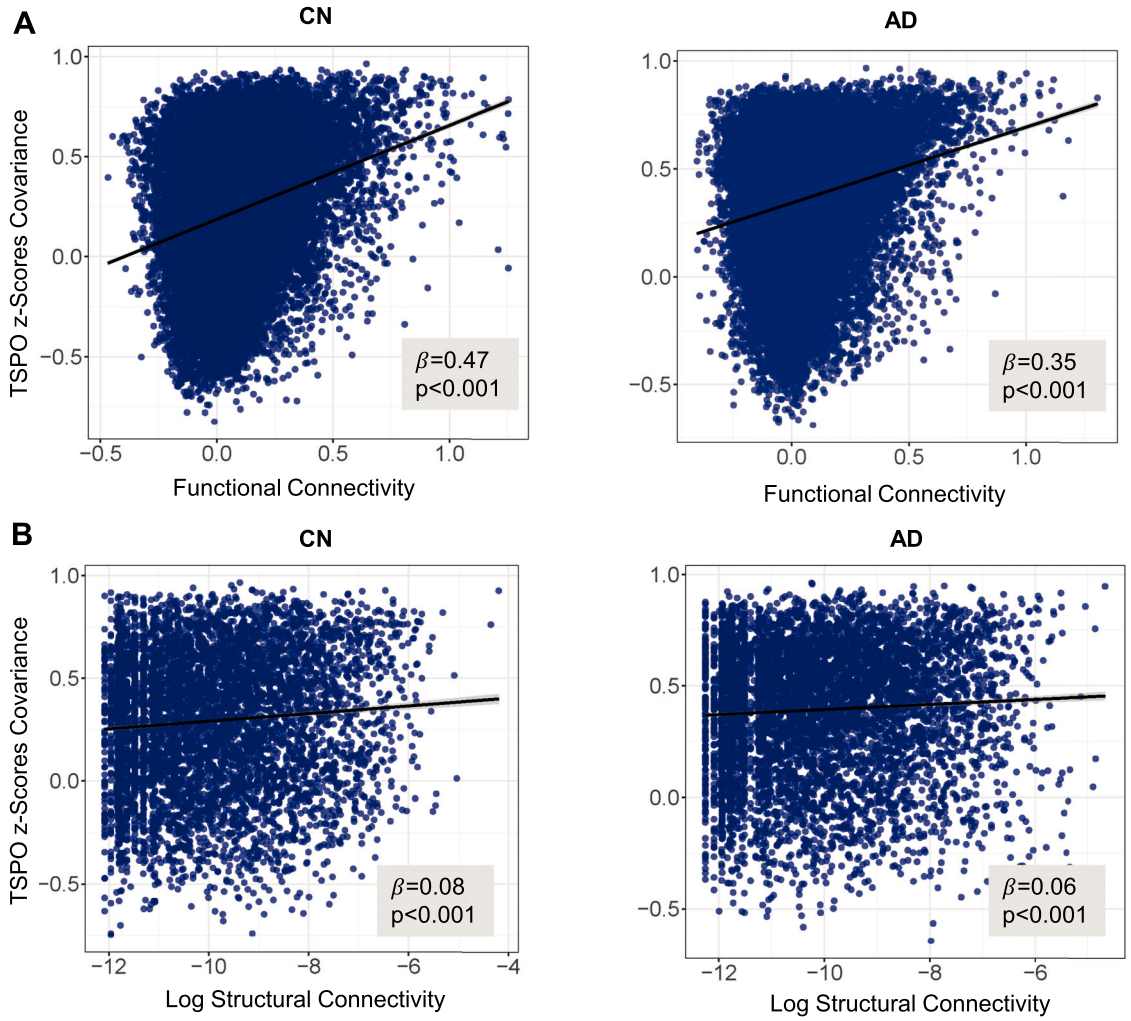

FIGURE 5: (A) Associations between functional connectivity and mitochondrial 18 kDa translocator protein (TSPO)–positron emission tomography (PET) microglial activation. (B) Associations between structural connectivity and TSPO-PET microglial activation. AD = Alzheimer disease; CN = cognitively normal controls; Log = logarithm.

correction for multiple comparisons, with a significance level of $p < 0.05$. Differences in structural connectivity between the diagnostic groups were tested in a general linear model using the individual DTI-derived adjacency matrices of the number of tracts comprising the 246 BN atlas-based regions in the GraphVar toolbox adjusted for age, sex, and education. Associations between clinical scores and TSPO-PET uptake were tested using a quadratic regression analysis in SPSS (SPSS Statistics for Windows, v26.0; IBM, Armonk, NY) assuming a disease stage-dependent microglial activation pattern, as shown previously.[15]

To assess the association between MRI functional/structural connectivity and microglial activation on PET, the Fisher *r*-to-*z* transformed matrices of functional connectivity and the *z*-transformed DTI-derived number of tracts matrices for each subject were used. First, the BN atlas-based TSPO-PET SUVR for each subject was concatenated, vectorized, and *z*-transformed to remove intersubject differences of the tracer uptake,[37] followed by a pairwise interregional correlation to calculate a TSPO-PET covariance adjacency matrix for each diagnostic group. We vectorized the TSPO-PET covariance matrix and the mean functional and structural connectivity adjacency matrices and performed a linear regression analysis to predict TSPO-PET covariance from connectivity. Due to skewed distribution, the vectorized structural connectivity was log-transformed for further analysis. The DTI-derived connectivity matrix exhibited a certain degree of sparsity with some brain regions not connected by fibre tracts, these brain regions were excluded. Second, we tested how depending on the TSPO-PET uptake in a seed region connectivity was associated with TSPO-PET uptake in the target regions. To this end, we first calculated the mean adjacency matrix of functional and structural connectivity, followed by correlating each mean matrix with the TSPO SUVR vector to obtain a correlation vector. Subsequently, in a linear regression analysis, we tested how the TSPO-PET SUVRs were associated with the correlation vectors between functional/structural connectivity and TSPO SUVR. Finally, the association between TSPO-PET uptake in functional/structural connectivity target regions and the functional/structural connectivity in hot spot and cold spot seed areas of TSPO-PET uptake was assessed. The mean TSPO

SUVR uptake was sorted discerningly in all 246 BN regions for each diagnostic group to define a hot and a cold spot region. Subsequently, in consequent regression analyses, the TSPO-PET uptake in all target regions was predicted by the functional/structural connectivity of the hot spot and cold spot. Visualizations of the results were performed using the R package ggplot2.

Results

Differences in sociodemographic and clinical data between the diagnostic groups are presented in the Table. There were no differences in age, sex, body weight, and years of education. Compared to cognitively normal controls, AD subjects had significantly ($p < 0.001$) worse cognitive performance (CERAD-NB and MMSE) and higher CDR Sum of the Boxes (SOB) ratings. As expected, AD patients showed more pathological CSF biomarker concentrations compared to the control group (lower Aβ42 and Aβ42/40 ratio, higher ptau181 and ttau). sTREM2 levels were higher in AD compared to controls, but this numerical difference did not reach statistical significance in an analysis of variance adjusted for age, sex, and education (see Table). We analyzed the association between TSPO-PET uptake and the CSF sTREM2 concentration. AD patients revealed a significant quadratic association between TSPO-PET tracer uptake in the above regions, identified as AD-specific sites of microglial activation, and CSF sTREM2 ($R^2 = 0.39$, $p < 0.02$); no association between the two variables was found for the cohort as a whole ($R^2 = 0.05$, $p < 0.49$) and in normal controls separately ($R^2 = 0.12$, $p < 0.48$; Fig 3).

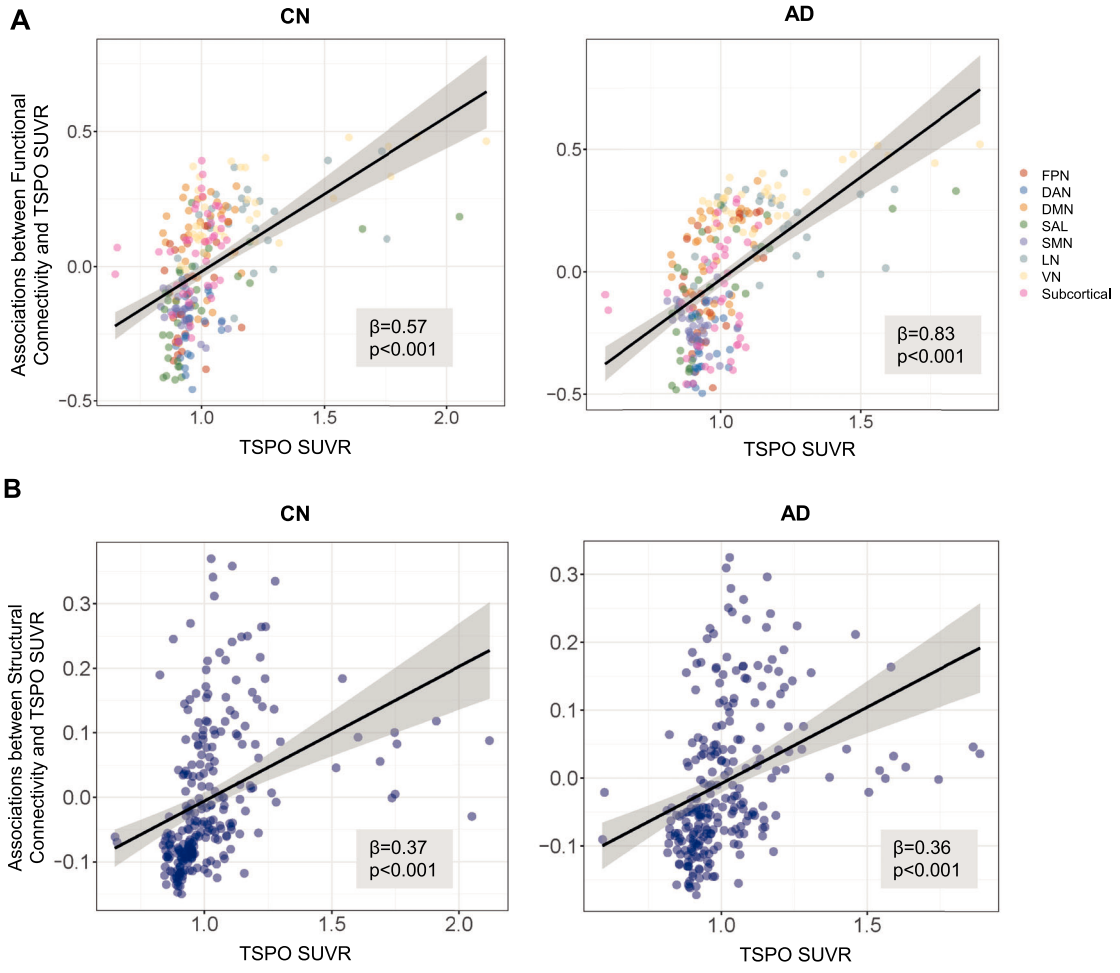

FIGURE 6: Connectivity is associated with mitochondrial 18 kDa translocator protein (TSPO)–positron emission tomography (PET) uptake in the target regions depending on TSPO-PET uptake in a seed region. The mean TSPO-PET uptake in the 246 Brainnetome (BN) regions of interest are shown on the x-axis, and the correlation between connectivity and TSPO-PET uptake in the 246 BN regions is shown on the y-axis. We tested in this analysis whether the level of microglial activation in a given region (seed) was predictive of microglial activation in a connected region (target). For regions with high microglial activation (seed) a higher functional connectivity was associated with higher microglial activation (target) and vice versa. (A) Associators for functional connectivity. (B) Associators for structural connectivity. AD = Alzheimer disease; CN = cognitively normal controls; DAN = dorsal attention network; DMN = default mode network; FPN = frontoparietal network; LN = limbic network; SAL= salience network; SMN = sensorimotor network; SUVR = standardized uptake value ratio; VN = visual network.

Differences between Patients and Controls on Imaging and Clinical Variables

Supporting the notion of increased microglial activation in AD, the Aβ-positive patient group showed increased TSPO-PET tracer uptake compared to Aβ-negative healthy control subjects in the bilateral anterior medial temporal lobe ($p < 0.001$; Fig 1A). In line with previous reports,[38,39] other than elevated TSPO-PET uptake levels in the inferior temporal gyrus/mesiotemporal, (pre)cuneus, and posterior cingulate regions, the mean TSPO-PET uptake was highest in the occipital region. In line with the view of AD as a network disorder, structural and functional connectivity were decreased on the whole brain level and within the default mode network comparing AD patients with healthy controls (results not shown). To link microglial activation with clinical outcomes, we analyzed how TSPO tracer uptake in the anterior medial temporal lobe was associated with dementia severity and cognitive impairment. Our analysis revealed a quadratic association between anterior medial temporal lobe TSPO-PET SUVR and CDR SOB ($R^2 = 0.39$, $p < 0.001$), CERAD-NB total score ($R^2 = 0.20$, $p < 0.017$), and MMSE score ($R^2 = 0.15$, $p = 0.049$; see Fig 3), suggesting an AD stage-dependent activation of the brain's immune system.

Associations between Functional and Structural Connectivity and TSPO-PET

To address our main hypothesis of a connectivity-based distribution of neuroinflammation, we assessed whether interconnected brain regions show covarying levels of microglial activation in AD patients. To this end, we obtained adjacency matrices of functional and structural connectivity using the 246 BN regions generated for the control and AD patient groups (Fig 4B, C). Using the same regions, TSPO-PET-derived covariance matrices were calculated for cognitively normal controls and AD patients (see Fig 4A). For comparison, the mean TSPO-PET SUVR binding pattern within the AD group is shown in Figure 1B. In a subsequent regression analysis, the associations of functional and structural connectivity with TSPO-PET tracer uptake covariance were assessed. Supporting our hypothesis, we found that more strongly interconnected brain regions showed a greater covariance in TSPO-PET in AD ($\beta = 0.35$, $p < 0.001$) and in the control group ($\beta = 0.47$, $p < 0.001$). Adjusting the analysis for sTREM2 concentration did not change the results (Fig 5A). For structural connectivity, a weak association with TSPO-PET covariance was shown for AD patients ($\beta = 0.06$, $p < 0.001$) and control subjects ($\beta = 0.06$; $p < 0.001$; see Fig 5B).

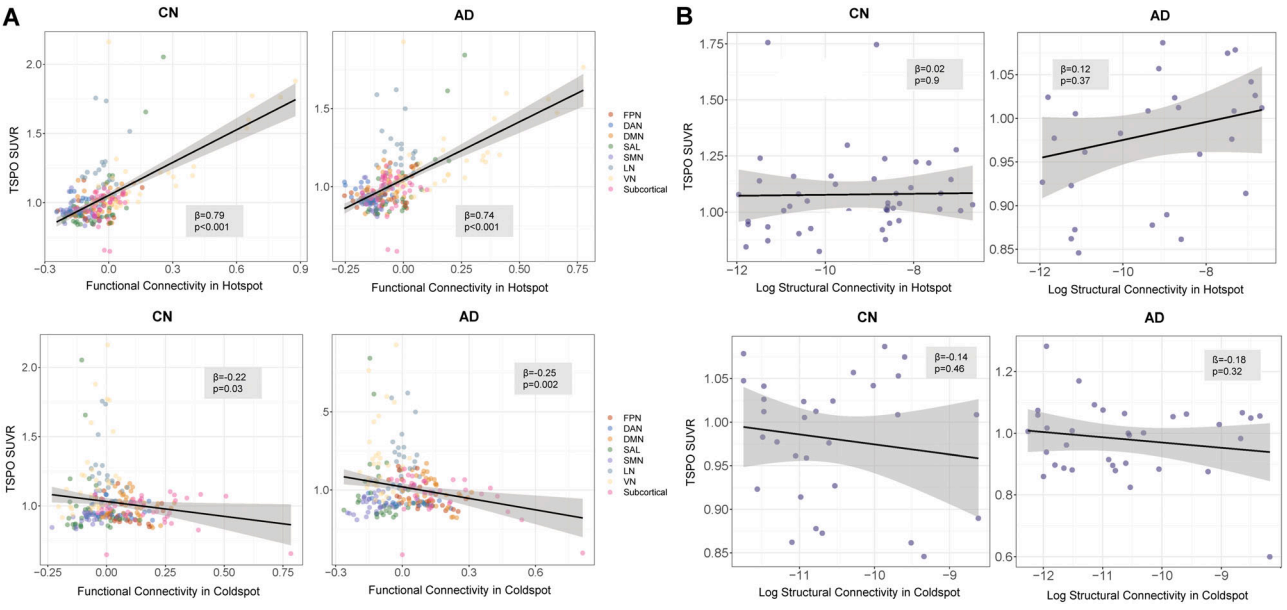

FIGURE 7: (A) Associations between mitochondrial 18 kDa translocator protein (TSPO)–positron emission tomography (PET) tracer uptake and functional connectivity in TSPO-PET hot spot in temporo-occipital (Brainnetome [BN] region 190) and TSPO-PET cold spot in the caudate nucleus/basal ganglia (BN regions 227/228). (B) Structural connectivity in TSPO-PET hot spot in temporo-occipital (BN region 190) and TSPO-PET cold spot in the caudate nucleus/basal ganglia (BN region 227/228). Functional connectivity of the hot spot and cold spot region with all remaining regions of the BN atlas is shown on the x-axis, and TSPO uptake in each region is shown on the y-axis. AD = Alzheimer disease; CN = cognitively normal controls; DAN = dorsal attention network; DMN = default mode network; FPN = frontoparietal network; LN = limbic network; Log = logarithm; SMN = sensorimotor network; SUVR = standardized uptake value ratio; VN = visual network.

Network Connectivity Prediction of TSPO-PET Tracer Uptake

We explored whether TSPO-PET tracer uptake in a particular region is predictive of the TSPO levels in a connected region, following a similar approach proposed recently for the association between functional connectivity and tau PET.[40] For seed regions with higher levels of TSPO-PET uptake, functional connectivity was associated with higher levels of TSPO-PET uptake in the target regions and vice versa in the AD group ($\beta = 0.83$, $p < 0.001$) and healthy controls ($\beta = 0.57$, $p < 0.001$; Fig 6A). A somewhat weaker association was shown for structural connectivity in both groups (AD: $\beta = 0.36$, $p < 0.001$; controls: $\beta = 0.37$, $p < 0.001$; see Fig 6B).

We analyzed how functional connectivity in seed regions with high TSPO-PET tracer uptake and in seed regions with low TSPO uptake was associated with the TSPO-PET uptake in all target regions. The target regions were defined by all other regions in the BN atlas except the hot spot and cold spot. The hot spot seed regions analysis revealed strong positive associations in cognitively normal controls ($\beta = 0.79$, $p < 0.001$) and AD patients ($\beta = 0.74$, $p < 0.001$), whereas in the cold spot seed regions analyses, a negative association was shown for both groups (cognitively normal controls: $\beta = -0.22$, $p < 0.03$; AD patients: $\beta = -0.25$, $p = 0.002$; Fig 7A). The same analysis based on structural connectivity did not reveal any significant positive or negative associations (see Fig 7B).

Discussion

Microglial activation is increasingly considered the third pathological hallmark of AD, in addition to Aβ and tau deposition.[41] The main objective of our study was to explore whether connectivity is associated with the patterns of microglial activation in patients with early AD and healthy control subjects, using the third-generation TSPO-PET tracer [^{18}F]GE-180. Our two key findings are that functional connectivity is associated spatially with microglial activation and we speculate that microglial activation spreads along pathways of highly connected brain regions, similar to the propagation pattern of tau pathology. We also show that microglial activation is increased in early AD subjects compared to healthy controls, predominantly in the temporal lobe, and that the association of TSPO-PET tracer uptake with clinical disease severity varies with disease stage, supporting a stage-specific role of the brain immune system. These findings are in line with several previous studies reporting early neurodegenerative and inflammatory changes in the medial temporal lobe,[42,43] overlapping with the earliest sites of tau pathology accumulation.[22] An AD stage-dependent behavior was earlier suggested for sTREM2 in CSF, another marker of microglial activation with an inverse U-shaped association with AD severity.[31,44] For TSPO-PET, this stage-dependent association was shown in a mouse model overexpressing the Aβ precursor protein.[15]

A growing body of evidence supports a model of prionlike tau spreading with progressing neurodegeneration, presumably promoted by neural activity.[18,40,45] We hypothesize that not only tau, but also microglial activation follows a distribution along functional connectivity pathways, in line with a spatial pathological colocalization. We report that brain areas with higher microglial activation show increased functional connectivity within the same region and with other regions with activated microglia. Previous research indicates that microglial activation is related to tau propagation and colocalization with tau pathology in a Braak stage-like fashion; furthermore, microglial activation was found to precede tau pathology.[20,21,46] Although the present study did not explore directly the spatial colocalization of microglial and tau tracer uptake on PET, the Braak stage-like pattern of neuroinflammatory response in early AD still suggests a close relationship between both pathologies. In support of this hypothesis, a recent multimodal study suggested a strong spatial overlap between tau and microglial PET as well as gray matter atrophy.[42]

We also observed that regions with low microglial activation showed decreased functional connectivity, supporting the hypothesis that not only tau but also activated microglia distributes along functionally connected brain areas. Because we observed weaker associations for structural connectivity, we argue that regions of neuroinflammation are connected by neural activity rather than simply by structural connections. Interestingly, the association between functional connectivity and microglial activation was somewhat weaker but similar in the AD group and in the normal controls. An inflammatory profile of the aged human brain has been demonstrated by molecular analysis, CSF, neuroimaging, and histological studies, suggesting enhanced microglial activation in healthy aging independently from Aβ pathology.[47] Furthermore, TSPO-PET uptake was shown to be associated with age, with increased uptake in healthy older participants.[48–50] In the analysis of the association between functional connectivity and microglial activation in the hot spots and cold spots, we observed a significant positive beta in the hot spot and a significant negative beta in the cold spot area; this is in line with the other analysis, suggesting that regions with low microglia activation are sparsely connected with other brain regions exhibiting lower microglial activation, whereas regions with high microglia activation seem to be highly connected with other regions exhibiting high microglia activation. These results further support the hypothesis of a connectivity-based distribution pattern. The observed

connectivity-based distribution pattern of microglial activation highlights the importance of an improved mechanistic understanding of spatial distribution of different pathologies across the brain, not limited to Aβ and tau. Strategies to reduce the neural activity-dependent propagation of AD pathology may be a promising avenue for future disease-modifying interventions. It remains to be shown that tau is the leading factor in this process of connectivity-dependent pathology spreading across the brain, followed by a reactive activation of microglia in the same regions. Microglia phagocytose tau and therefore might play an important role in spreading of tau pathology throughout the brain.[51,52] There is also evidence that an interaction between microglial activation and Aβ triggers the dissemination of tau across the Braak stages.[21] Another speculative mechanism of the observed associations between functional connectivity and microglia activation refers to synaptic pruning, an essential mechanism in healthy brain development.[53] Askew pruning in AD and age-related diseases by microglia, normally confined to brain development, might result in synaptic loss during adulthood and drive the observed connectivity changes.[54,55] Recently, it has been shown that microglia is directly involved in the regulation of neural activity, providing a negative feedback mechanism operating similarly to inhibitory neurons.[56] One might speculate that failure in this direct regulation of neural activity by microglia results in the observed changes in functional connectivity associated with microglial activity. Further studies including both tau and microglia PET should address the question of possible differences in the sequence of tau and inflammation distribution. The 18-month follow-up assessments of the ActiGliA participants include [^{18}F]PI2620 tau-PET, allowing us to address this question in our cohort in the future.

There are potential limitations of this study. A relatively small sample size restricts the statistical power of some of the analyses, but previous studies relied on cohorts of comparable size,[57] and the presented data are of explorative nature and should be confirmed in independent datasets. The small sample size may also be the reason for the nonsignificant group differences for CSF sTREM2. However, to the best of our knowledge, the assessed cohort is the largest and best characterized dataset of its kind with both TSPO and amyloid PET, CSF biomarkers, and resting-state fMRI available for all participants. No pathological verification was available to confirm the clinical diagnoses; however, a careful biomarker-based stratification and in-depth phenotyping minimizes the likelihood of diagnostic misclassification. Limited blood–brain barrier passing of [^{18}F]GE-180 needs to be acknowledged, but our previous data indicated strong agreement with immunohistochemistry in AD models[58] and patterns matching known topology of microglial activation in neurodegenerative diseases.[10,59] The low background signal of [^{18}F]GE-180 appears to facilitate sensitive detection of alterations as a specific surrogate of microglial activation.[60,61] As a limitation of the quantification approach of TSPO-PET, we note that late static SUVRs were calculated with an intracerebral reference tissue. Although late static SUVRs showed suitability for TSPO-PET quantification,[62] this method was inferior to scaling by a late-tissue-to-blood ratio. Thus, we acknowledge that our quantification approach may be subject to some bias by cerebral blood flow alterations and attenuation of a polymorphism effect. Lastly, AD patients were predominantly in an early disease stage, and group differences of microglial activation may have been diluted in the cross-sectional analysis if several activity peaks exist as AD progresses.[63] Despite lack of a significant difference in sTREM2 between the two diagnostic groups, a quadratic association between sTREM2 concentration and TSPO-PET uptake was revealed. A similar pattern was found in our previous study in 4-repeat tauopathies,[10] where we interpreted these observations as an indication of a functional burnout of microglia with increasing activity. The same hypothesis may apply here but needs further verification in longitudinal analyses.

To conclude, the results of our study suggest that neuroinflammation is related to microglial activation in AD and we speculate that it spreads along highly connected brain regions. It remains to be explored whether this pattern reflects a consequence of transneuronal tau spreading or whether neuroinflammation itself promotes tau distribution. We confirm that clinical expression of AD pathology is affected by neuroinflammation, and our findings raise the important question of whether anti-inflammatory treatments could modify transneural transmission, emphasizing the need for further comprehensive research integrating mechanisms on the molecular and macro-scale brain network levels.

Acknowledgments

This study was supported by the German Center for Neurodegenerative Disorders (Deutsches Zentrum für Neurodegenerative Erkrankungen), Hirnliga (Manfred-Strohscheer Stiftung), and the German Research Foundation (Deutsche Forschungsgemeinschaft) under Germany's Excellence Strategy within the framework of the Munich Cluster for Systems Neurology (EXC 2145 SyNergy, ID 390857198). The authors thank Christian Haass, PhD for his support. Open Access funding enabled and organized by Projekt DEAL.

Author Contributions

B.-S.R., M.B., J.L., G.H., and R.P. contributed to the conception and design of the study; B.-S.R., M.B., R.P., N.F., L.T., M.Z., E.E., E.M.-R., S.G., L.B., C.K., J.H., M.T., J.U., B.P., O.P., D.J., K.B., M.E., C.P., E.W., G.B., S.Sc., A.F., F.E., R.R., A.R., O.G., T.G., D.K., S.St., O.D., and P.B. contributed to the acquisition and analysis of data; B.-S.R., M.B., N.F., L.T., M.Z., and R.P. contributed to drafting the text or preparing the figures.

Potential Conflicts of Interest

Nothing to report.

References

1. Hardy JA, Higgins GA. Alzheimer's disease: the amyloid cascade hypothesis. Science 1992;256:184–185.
2. Calsolaro V, Edison P. Neuroinflammation in Alzheimer's disease: current evidence and future directions. Alzheimers Dement 2016;12:719–732.
3. Heneka MT, Carson MJ, El Khoury J, et al. Neuroinflammation in Alzheimer's disease. Lancet Neurol 2015;14:388–405.
4. Rauchmann B-S, Sadlon A, Perneczky R. Alzheimer's Disease Neuroimaging Initiative. Soluble TREM2 and inflammatory proteins in Alzheimer's disease cerebrospinal fluid. J Alzheimers Dis 2020;73:1615–1626.
5. Rauchmann B-S, Schneider-Axmann T, Alexopoulos P, et al. CSF soluble TREM2 as a measure of immune response along the Alzheimer's disease continuum. Neurobiol Aging 2019;74:182–190.
6. Shen X-N, Niu L-D, Wang Y-J, et al. Inflammatory markers in Alzheimer's disease and mild cognitive impairment: a meta-analysis and systematic review of 170 studies. J Neurol Neurosurg Psychiatry 2019;90:590–598.
7. Itagaki S, McGeer PL, Akiyama H, et al. Relationship of microglia and astrocytes to amyloid deposits of Alzheimer disease. J Neuroimmunol 1989;24:173–182.
8. Edison P, Brooks DJ. Role of neuroinflammation in the trajectory of Alzheimer's disease and in vivo quantification using PET. J Alzheimers Dis 2018;64:S339–S351.
9. Knezevic D, Mizrahi R. Molecular imaging of neuroinflammation in Alzheimer's disease and mild cognitive impairment. Prog Neuropsychopharmacol Biol Psychiatry 2018;80:123–131.
10. Palleis C, Sauerbeck J, Beyer L, et al. In vivo assessment of neuroinflammation in 4-repeat tauopathies. Mov Disord 2021;36:883–894.
11. Gerrits E, Brouwer N, Kooistra SM, et al. Distinct amyloid-β and tau-associated microglia profiles in Alzheimer's disease. Acta Neuropathol 2021;141:681–696.
12. Hayes A, Thaker U, Iwatsubo T, et al. Pathological relationships between microglial cell activity and tau and amyloid beta protein in patients with Alzheimer's disease. Neurosci Lett 2002;331:171–174.
13. Dani M, Wood M, Mizoguchi R, et al. Microglial activation correlates in vivo with both tau and amyloid in Alzheimer's disease. Brain 2018;141:2740–2754.
14. Plescher M, Seifert G, Hansen JN, et al. Plaque-dependent morphological and electrophysiological heterogeneity of microglia in an Alzheimer's disease mouse model. Glia 2018;66:1464–1480.
15. Blume T, Focke C, Peters F, et al. Microglial response to increasing amyloid load saturates with aging: a longitudinal dual tracer in vivo μPET-study. J Neuroinflammation 2018;15:307.
16. Kitazawa M, Yamasaki TR, LaFerla FM. Microglia as a potential bridge between the amyloid beta-peptide and tau. Ann N Y Acad Sci 2004;1035:85–103.
17. Cope TE, Rittman T, Borchert RJ, et al. Tau burden and the functional connectome in Alzheimer's disease and progressive supranuclear palsy. Brain 2018;141:550–567.
18. Franzmeier N, Neitzel J, Rubinski A, et al. Functional brain architecture is associated with the rate of tau accumulation in Alzheimer's disease. Nat Commun 2020;11:347.
19. Vogel JW, Iturria-Medina Y, Strandberg OT, et al. Spread of pathological tau proteins through communicating neurons in human Alzheimer's disease. Nat Commun 2020;11:2612.
20. Hopp SC, Lin Y, Oakley D, et al. The role of microglia in processing and spreading of bioactive tau seeds in Alzheimer's disease. J Neuroinflammation 2018;15:269.
21. Pascoal TA, Benedet AL, Ashton NJ, et al. Microglial activation and tau propagate jointly across Braak stages. Nat Med 2021;27:1592–1599.
22. Braak H, Alafuzoff I, Arzberger T, et al. Staging of Alzheimer disease-associated neurofibrillary pathology using paraffin sections and immunocytochemistry. Acta Neuropathol 2006;112:389–404.
23. Jessen F, Spottke A, Boecker H, et al. Design and first baseline data of the DZNE multicenter observational study on predementia Alzheimer's disease (DELCODE). Alzheimers Res Ther 2018;10:15.
24. Schmitt J, Palleis C, Sauerbeck J, et al. Dual-phase β-amyloid PET captures neuronal injury and amyloidosis in corticobasal syndrome. Front Aging Neurosci 2021;13:661284.
25. Chandler MJ, Lacritz LH, Hynan LS, et al. A total score for the CERAD neuropsychological battery. Neurology 2005;65:102–106.
26. Fillenbaum GG, van Belle G, Morris JC, et al. Consortium to establish a registry for Alzheimer's disease (CERAD): the first twenty years. Alzheimers Dement 2008;4:96–109.
27. Folstein MF, Folstein SE, McHugh PR. "Mini-mental state". A practical method for grading the cognitive state of patients for the clinician. J Psychiatr Res 1975;12:189–198.
28. Kreisl WC, Jenko KJ, Hines CS, et al. A genetic polymorphism for translocator protein 18 kDa affects both in vitro and in vivo radioligand binding in human brain to this putative biomarker of neuroinflammation. J Cereb Blood Flow Metab 2013;33:53–58.
29. Vettermann FJ, Harris S, Schmitt J, et al. Impact of TSPO receptor polymorphism on [^{18}F]GE-180 binding in healthy brain and pseudoreference regions of neurooncological and neurodegenerative disorders. Life (Basel) 2021;11:484.
30. Dumurgier J, Schraen S, Gabelle A, et al. Cerebrospinal fluid amyloid-β 42/40 ratio in clinical setting of memory centers: a multicentric study. Alzheimers Res Ther 2015;7:30.
31. Suárez-Calvet M, Kleinberger G, Araque Caballero MÁ, et al. sTREM2 cerebrospinal fluid levels are a potential biomarker for microglia activity in early-stage Alzheimer's disease and associate with neuronal injury markers. EMBO Mol Med 2016;8:466–476.
32. Leemans A, Jeurissen B, Sijbers J, Jones DK. ExploreDTI: a graphical toolbox for processing, analyzing, and visualizing diffusion MR data. 2009. Available at: https://www.semanticscholar.org/paper/f92f4418d4a4523a5760414144ecce8ab6472fde. Accessed September 2, 2021.
33. Baker SL, Maass A, Jagust WJ. Considerations and code for partial volume correcting [^{18}F]-AV-1451 tau PET data. Data Brief 2017;15:648–657.
34. Brendel M, Barthel H, van Eimeren T, et al. Assessment of 18F-PI-2620 as a biomarker in progressive supranuclear palsy. JAMA Neurol 2020;77:1408–1419.
35. Fan L, Li H, Zhuo J, et al. The human Brainnetome atlas: a new brain atlas based on connectional architecture. Cereb Cortex 2016;26:3508–3526.

36. Kruschwitz JD, List D, Waller L, et al. GraphVar: a user-friendly toolbox for comprehensive graph analyses of functional brain connectivity. J Neurosci Methods 2015;245:107–115.

37. Veronese M, Moro L, Arcolin M, et al. Covariance statistics and network analysis of brain PET imaging studies. Sci Rep 2019;9:2496.

38. Kreisl WC, Lyoo CH, McGwier M, et al. In vivo radioligand binding to translocator protein correlates with severity of Alzheimer's disease. Brain 2013;136:2228–2238.

39. Fan Z, Okello AA, Brooks DJ, Edison P. Longitudinal influence of microglial activation and amyloid on neuronal function in Alzheimer's disease. Brain 2015;138:3685–3698.

40. Franzmeier N, Rubinski A, Neitzel J, et al. Functional connectivity associated with tau levels in ageing, Alzheimer's, and small vessel disease. Brain 2019;142:1093–1107.

41. Kinney JW, Bemiller SM, Murtishaw AS, et al. Inflammation as a central mechanism in Alzheimer's disease. Alzheimers Dement 2018;4:575–590.

42. Su L, Surendranathan A, Huang Y, et al. Relationship between tau, neuroinflammation and atrophy in Alzheimer's disease: the NIMROD study. Inf Fusion 2021;67:116–124.

43. Khan UA, Liu L, Provenzano FA, et al. Molecular drivers and cortical spread of lateral entorhinal cortex dysfunction in preclinical Alzheimer's disease. Nat Neurosci 2014;17:304–311.

44. Suárez-Calvet M, Morenas-Rodríguez E, Kleinberger G, et al. Early increase of CSF sTREM2 in Alzheimer's disease is associated with tau related-neurodegeneration but not with amyloid-β pathology. Mol Neurodegener 2019;14:1.

45. Pereira JB, Ossenkoppele R, Palmqvist S, et al. Amyloid and tau accumulate across distinct spatial networks and are differentially associated with brain connectivity. Elife 2019;8:e50830.

46. Serrano-Pozo A, Mielke ML, Gómez-Isla T, et al. Reactive glia not only associates with plaques but also parallels tangles in Alzheimer's disease. Am J Pathol 2011;179:1373–1384.

47. Niraula A, Sheridan JF, Godbout JP. Microglia priming with aging and stress. Neuropsychopharmacology 2017;42:318–333.

48. Gulyás B, Vas A, Tóth M, et al. Age and disease related changes in the translocator protein (TSPO) system in the human brain: positron emission tomography measurements with [11C]vinpocetine. Neuroimage 2011;56:1111–1121.

49. Schuitemaker A, van der Doef TF, Boellaard R, et al. Microglial activation in healthy aging. Neurobiol Aging 2012;33:1067–1072.

50. Tuisku J, Plavén-Sigray P, Gaiser EC, et al. Effects of age, BMI and sex on the glial cell marker TSPO—a multicentre [^{11}C]PBR28 HRRT PET study. Eur J Nucl Med Mol Imaging 2019;46:2329–2338.

51. Asai H, Ikezu S, Tsunoda S, et al. Depletion of microglia and inhibition of exosome synthesis halt tau propagation. Nat Neurosci 2015;18:1584–1593.

52. Vogels T, Murgoci A-N, Hromádka T. Intersection of pathological tau and microglia at the synapse. Acta Neuropathol Commun 2019;7:109.

53. Paolicelli RC, Bolasco G, Pagani F, et al. Synaptic pruning by microglia is necessary for normal brain development. Science 2011;333:1456–1458.

54. Paolicelli RC, Jawaid A, Henstridge CM, et al. TDP-43 depletion in microglia promotes amyloid clearance but also induces synapse loss. Neuron 2017;95:297–308.e6.

55. Subramanian J, Savage JC, Tremblay M-È. Synaptic loss in Alzheimer's disease: mechanistic insights provided by two-photon in vivo imaging of transgenic mouse models. Front Cell Neurosci 2020;14:592607.

56. Badimon A, Strasburger HJ, Ayata P, et al. Negative feedback control of neuronal activity by microglia. Nature 2020;586:417–423.

57. Völk S, Unterrainer M, Albert NL, et al. TSPO PET with 18F-GE-180 to differentiate variants of multiple sclerosis: relapsing-remitting multiple sclerosis, tumefactive demyelination, and Baló's concentric sclerosis. Clin Nucl Med 2020;45:e447–e448.

58. Parhizkar S, Arzberger T, Brendel M, et al. Loss of TREM2 function increases amyloid seeding but reduces plaque-associated ApoE. Nat Neurosci 2019;22:191–204.

59. Xiang X, Wind K, Wiedemann T, et al. Microglial activation states drive glucose uptake and FDG-PET alterations in neurodegenerative diseases. Sci Transl Med 2021;13:eabe5640.

60. Sridharan S, Raffel J, Nandoskar A, et al. Confirmation of specific binding of the 18-kDa translocator protein (TSPO) radioligand [^{18}F]GE-180: a blocking study using XBD173 in multiple sclerosis normal appearing white and grey matter. Mol Imaging Biol 2019;21:935–944.

61. Biechele G, Blume T, Deussing M, et al. Pre-therapeutic microglia activation and sex determine therapy effects of chronic immunomodulation. Theranostics 2021;11:8964–8976.

62. Kreisl WC, Henter ID, Innis RB. Imaging translocator protein as a biomarker of neuroinflammation in dementia. Adv Pharmacol 2018;82:163–185.

63. Fan Z, Brooks DJ, Okello A, Edison P. An early and late peak in microglial activation in Alzheimer's disease trajectory. Brain 2017;140:792–803.